journal

J. Am. Ceram. Soc., 72 [5] 746-53 (1989)

Debonding Properties of Residually Stressed Brittle-Matrix Composites

P. G. Charalambides and Anthony G. Evans*

Materials Department, College of Engineering, University of California, Santa Barbara, California 93106

Trends in interface debonding have been calculated during fiber pullout for composites with interfaces subject to residual tension. The debond behavior is shown to depend sensitively on the thermal expansion mismatch. The results are used as the basis for designing a pullout test specimen suitable for measuring the mixed-mode fracture energy of bimaterial interfaces. The solutions also provide the background needed to assess the role of debonding in the toughening of ceramics by fibers. [Key words: composites, fracture, interfaces, mechanical properties, fibers.]

I. Introduction

EXPERIMENTAL observations reported in companion studies[1,2] suggest that, in an important class of tough ceramic composites, a low fracture resistance interface exists with interfaces subject to residual *tension*, such that partial debonding occurs on cooling. When the matrix crack front approaches the fiber, the initial debonds extend along the interface (Appendix A) and inhibit fiber failure (Fig. 1).[3] Many of the fibers thus remain intact and allow toughening by bridging and pullout.[4]

Understanding of the subsequent events involved in fiber failure can be achieved by analyzing the behavior of debond cracks, as the intact fibers are axially loaded in the crack wake between the crack surfaces (Fig. 1). One of the important issues concerns the ability of the interface to further debond in the crack wake. The incidence and extent of such debonding has a strong influence on the stress in the fiber and thus on pullout toughening, through the influence of this stress on the location of fiber failure.[4] In order to address this issue, the stress and displacement fields near the debond tip, as well as relationships with the critical values for debond growth, are required. Some basic mechanics of interface cracks[5-7] (Appendix B) indicate that this problem can be studied by using the crack tip stresses and displacements to calculate the strain energy release rate $\mathcal{G}$ and the phase angle of loading, ψ, at the debond (Appendix B). The latter is a measure of the mixity of opening and shear along the surface of the debond crack. A numerical method is used in the present study to calculate both $\mathcal{G}$ and ψ.

Further background is provided by recent investigations of the fracture energy of interfaces,[7,8] $\mathcal{G}_{ic}$, which indicate that such fracture can be characterized by a locus involving $\mathcal{G}_{ic}$ and ψ. Moreover, for *all-brittle* constituents, $\mathcal{G}_{ic}$ typically becomes large as $\psi \rightarrow \pi/2$ (Fig. 2),[8] because of asperity contacts on the debond surfaces within a bridging zone near the debond tip. Evaluation of the phase angle thus emerges as a vitally important aspect of the study. Such analysis is performed in the conventional manner by ignoring the shear tractions that exist along asperity contacts in the bridging zone. Then the frictional contacts govern the fracture $\mathcal{G}_{ic}(\psi)$, but do not enter the mechanics.

Several other phenomena having importance for composites are also examined using the present analysis. First, the calculation of $\mathcal{G}$ and ψ can be used to interpret *pullout experiments* which are designed to *measure* the debond fracture energy, $\mathcal{G}_{ic}$, at large values of the phase angle. Furthermore, the magnitudes of $\mathcal{G}$ and ψ also provide the basis for determining whether fibers are able to fail from the end of the debond rather than within the debond length, by weakest-link statistics. Understanding of these fiber failure possibilities is critical to the analysis of pullout toughing.[4] Finally, analysis of the compliance of debonded fibers provides new insight about the bridging contribution to toughness.

G. L. Messing—contributing editor

Manuscript No. 199284. Received February 25, 1988; approved October 3, 1988.
Supported by the Defense Advanced Research Projects Agency (DARPA) University Research Initiative (URI) at the University of California, Santa Barbara, under Contract No. N00014-86-K-0753.
*Member, American Ceramic Society.

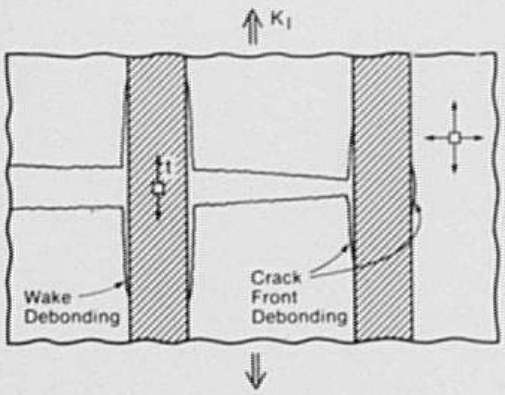

Fig. 1. Schematic diagram indicating crack front and wake debonding in fiber-reinforced ceramics.

II. Debonding Mechanics

(1) Stress-Free Composites

The stress on a debonded fiber caused by matrix opening results in a stress intensification at the end of the debond such that, in the absence of contacting asperities, steady-state conditions ($\mathcal{G}$ independent of debond length) must obtain when the debond length is somewhat larger than the fiber radius. Furthermore, *in the absence of residual stress*, the approximate steady-state strain energy release rate $\mathcal{G}$ can be analytically derived. This is achieved for the composite cylinder shown in Fig. 2(A) by noting that the axial stresses are substantially larger than the radial and tangential stresses, whereupon $\mathcal{G}$ is closely related to the strain energies, U, in regions (i) and (ii) of Fig. 2(B) by

$$\mathcal{G} = (U_i - U_{ii})/2\pi a \Delta \ell \tag{1}$$

where a is the fiber radius and $\Delta\ell$ is an increment in debond length (Fig. 2(B)). It is straightforward to derive the strain energies as

$$U_i = \frac{\pi a^2 \Delta \ell}{2E_f} t^2 \tag{2a}$$

$$U_{ii} = \frac{\pi a^2 \Delta \ell}{2E_f}\left[\left(\frac{\sigma_f}{t}\right)^2 + \frac{1-f}{f}\frac{E_f}{E_m}\left(\frac{\sigma_m}{t}\right)^2\right] t^2 \tag{2b}$$

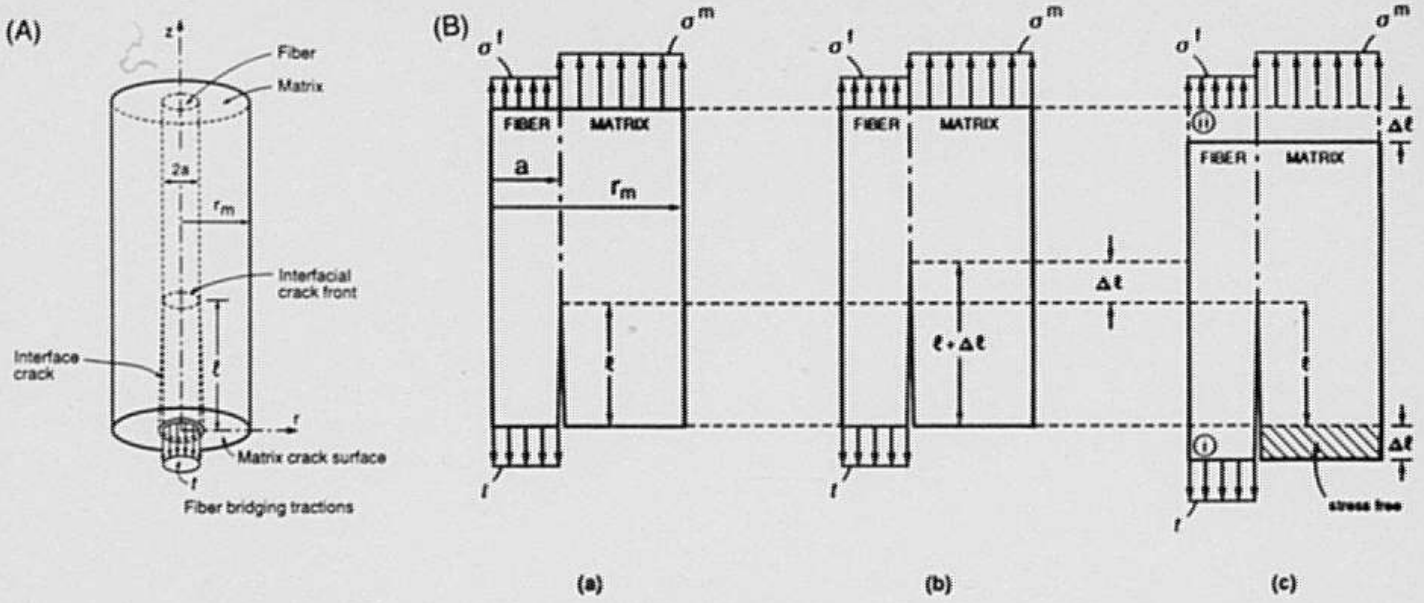

Fig. 2. (A) The composite cylinder used for analysis and (B) the regions of stress release in steady state.

where E is Young's modulus,[†] and the stresses σ_f and σ_m are given by

$$\sigma_f = \frac{f}{f + \Sigma(1-f)}t$$

$$\sigma_m = \frac{f\Sigma}{f + \Sigma(1-f)}t$$

with $\Sigma = E_m/E_f$. Inserting U from Eqs. (2) into Eq. (1) gives

$$\frac{\mathcal{G}E_f}{t^2a} = \frac{1}{4}\frac{\Sigma}{\Sigma + \dfrac{f}{1-f}} \tag{3}$$

It is noted that in bimaterial systems with equal Poisson's ratios (i.e., $\nu_f = \nu_m$) loaded with an axial stress t, the interface pressure and therefore the radial and tangential stresses are zero. In this instance, the expression for $\mathcal{G}$ given by Eq. (3) is exact. The trends in nondimensional $\mathcal{G}$ are plotted in Fig. 3.

Further progress is achieved by numerically evaluating the strain energy release rate and the phase angle at the debond front, using a finite-element procedure developed for interface cracks[9] (Appendix C). The finite-element equations were solved for the fiber/matrix unit-cell boundary value problem shown in Fig. 2(A). Because of the axisymmetry of the problem, it is sufficient to solve the finite-element equations in only a radial plane of the unit cell. A typical finite-element mesh with the boundary conditions is depicted in Fig. 4. The results of the finite-element calculations are summarized in Figs. 3, 5, and 6.[‡] *Steady-state* conditions are confirmed when the debond length $\ell \geq a$ (Fig. 2(A)) such that the steady-state nondimensional strain energy release rates, $E_f\mathcal{G}/t^2a$, agree closely with the analytical solutions (Fig. 3). The steady-state phase angles are strong functions of the relative modulus, E_f/E_m, and of the relative Poisson ratio ν_f/ν_m. It is convenient to express these trends by means of a nondimensional phase angle, ψ^* (Appendix B), as depicted in Fig. 6 and Table I. The phase angle is typically large ($\psi^* > 1$), indicative of large relative shear displacements along the debond surfaces. It is also noted that $\mathcal{G}$ has a finite value at $\ell = 0$, governed by the *matrix crack* singularity. The associated nondimensional $\mathcal{G}$ for the homogeneous material is 0.06,[10] consistent with the present calculations (Fig. 5).

[†]Henceforth, the subscripts f and m will be used to represent quantities relevant to the fiber and matrix, respectively.

[‡]These results correspond to a crack tip system (see Fig. B1) where the *matrix* is taken as *material 1* and the *fiber* as *material 2*.

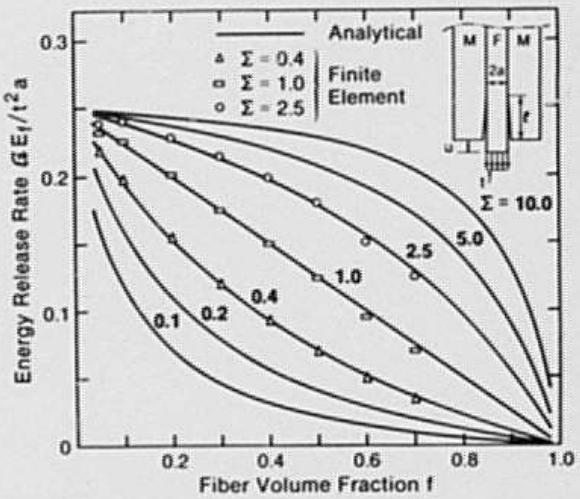

Fig. 3. Trends in steady-state strain energy release rate with volume fraction: both approximate analytical and numerical results are plotted. The numerical results were obtained for Poisson's ratios $\nu_f = \nu_m = 0.25$: $\Sigma = E_m/E_f$.

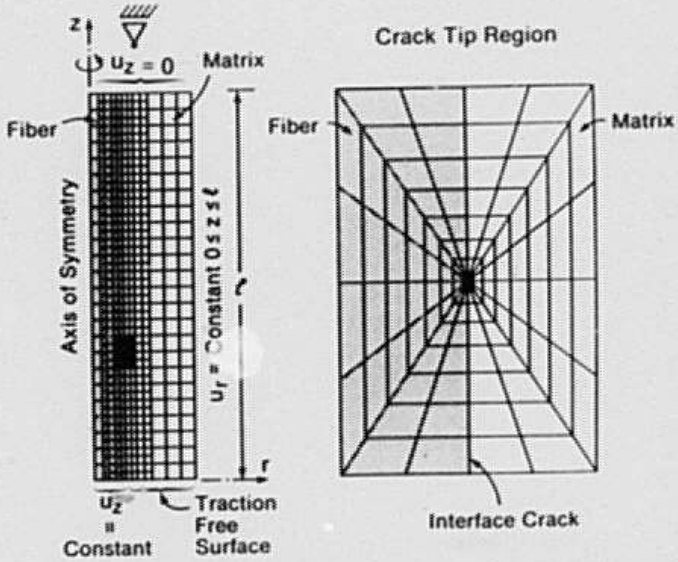

Fig. 4. Typical finite-element mesh and the boundary conditions used in solving the problem shown in Fig. 2(A).

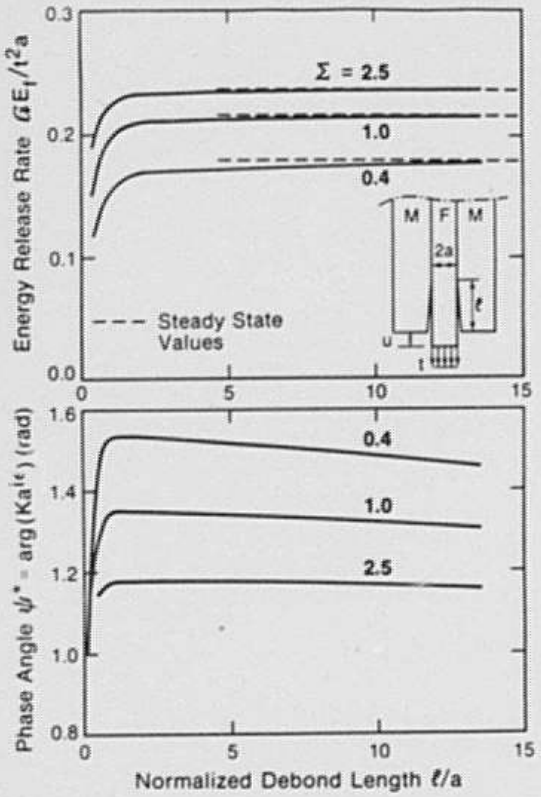

Fig. 5. Nondimensional strain energy release rate $\mathcal{G}E_f/t^2a$ and nondimensional phase angle, ψ^*: trends with debond length ℓ/a for a fiber volume fraction $f = 0.15$ and Poisson's ratios $\nu_f = \nu_m = 0.25$.

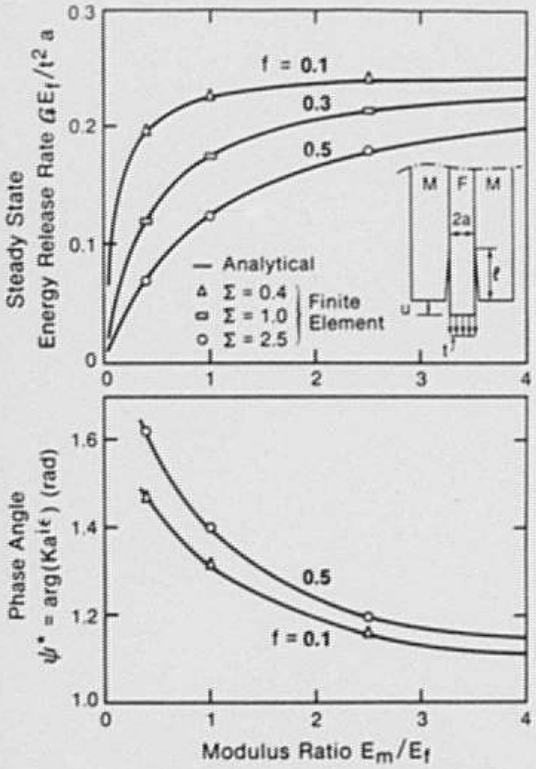

Fig. 6. Nondimensional strain energy releases rate and phase angle: trends with modulus ratio and volume fraction for $\nu_f = \nu_m = 0.25$.

Table I. Poisson's Ratio Effects on the Stress Intensities at the Crack Tip of a Debonded Fiber, $E_m/E_f = 1$

f	ν_f	ν_m	$\frac{\text{Re}\,(Ka^{i\varepsilon})}{t\sqrt{a}}$	$\frac{\text{Im}\,(Ka^{i\varepsilon})}{t\sqrt{a}}$	$\frac{E_f\mathcal{G}}{at^2}$	$\frac{E_f u}{at}$
0.15	0.3	0.2	0.132	0.461	0.215	10.5
0.15	0.25	0.25	0.117	0.463	0.214	10.5
0.15	0.2	0.3	0.106	0.467	0.214	10.5
0.30	0.3	0.2	0.112	0.419	0.176	10.2
0.30	0.25	0.25	0.094	0.421	0.175	10.2
0.30	0.2	0.3	0.079	0.426	0.175	10.3
0.50	0.3	0.2	0.079	0.357	0.125	9.9
0.50	0.25	0.25	0.060	0.358	0.124	10.0
0.50	0.2	0.3	0.044	0.362	0.124	10.0

(2) Residually Stressed Composites

When the thermal expansion coefficient of the fiber, α_f, exceeds that of the matrix, α_m, the interface is subject to residual tension upon cooling and the debond energy release rates are enhanced. These energy release rates can be calculated by noting that the stress intensities from the applied loads, and from the residual field, can be linearly superposed. The stress intensities in steady state provided by the residual and applied fields have thus been calculated using finite elements[9] (Appendix C) with the boundary adjusted to ensure that the shrinkage of the unit cell shown in Fig. 2(A) is compatible with its neighboring cells. For an elastically homogeneous composite ($\Sigma = 1$), the net stress intensities K^T on the stressed fibers in the matrix crack wake are

$$\frac{K_I^T}{E\Delta\alpha\Delta T\sqrt{a}} = 0.28 + 0.11\tau \tag{4a}$$

$$\frac{K_{II}^T}{E\Delta\alpha\Delta T\sqrt{a}} = -0.51 + 0.45\tau \tag{4b}$$

where $\Delta\alpha = \alpha_f - \alpha_m$ and ΔT is negative and $\tau = t/E\Delta\alpha\Delta T$. Corresponding results for composites having inhomogeneous elastic properties can be expressed in general by

$$\frac{\text{Re}\,(K^T a^{i\varepsilon})}{E_f\Delta\alpha\Delta T\sqrt{a}} = c_1 + c_2\tau_f \tag{5a}$$

$$\frac{\text{Im}\,(K^T a^{i\varepsilon})}{E_f\Delta\alpha\Delta T\sqrt{a}} = c_3 + c_4\tau_f \tag{5b}$$

where $\tau_f = t/E_f\Delta\alpha\Delta T$, Re and Im refer to the real and imaginary components of K, respectively (Appendix B), and the coefficients c_i depend on the elastic properties, as summarized in Table II. The results can now be expressed in terms of a strain energy release rate $\mathcal{G}^T/E_f a(\Delta\alpha\Delta T)^2$ and the nondimensional phase angle, ψ^* (Appendix B), as

$$\frac{\mathcal{G}^T}{E_f a(\Delta\alpha\Delta T)^2} = k_1 + k_2\tau_f + k_3\tau_f^2 \tag{6a}$$

$$\psi^* = \arctan\left[\frac{\text{Re}\,(K^T a^{i\varepsilon})}{\text{Im}\,(K^T a^{i\varepsilon})}\right] = h(\tau_f) \tag{6b}$$

with k_i being the coefficients presented in Table II, leading to the trend in $\mathcal{G}^T$ plotted in Fig. 7(A); ψ^* is the function plotted in Fig. 7(B). Several aspects of the results are noteworthy. Before a stress t is applied, $\mathcal{G}$ has a residual value and a large negative phase angle. Application of stress initially causes $\mathcal{G}$ to decrease, because the phase angle governed by the applied loading and the residual field have opposite sign. Consequently, ψ^* changes sign from negative to positive at a stress $t \approx E_f\Delta\alpha\Delta T$. As t becomes larger than $E_f\Delta\alpha\Delta T$, $\mathcal{G}$ increases monotonically with t, and when $t \geq 5E_f\Delta\alpha\Delta T$, $\mathcal{G}$ has essentially the value expected from the applied load alone (Eqs. (6)).

III. Crack Surface Compliances

The relationship between the fiber tractions, t, and the crack opening, u, which governs the bridging contribution to toughness[4] can also be deduced from the numerical results, as summarized in Fig. 8. Linear behavior obtains, as expected for steady state, such that in the absence of residual stress

$$\frac{uE_f}{ta} = \lambda_1(f,\Sigma) + \lambda_2(\Sigma)\frac{\ell}{a} \tag{7}$$

where λ_i ($i = 1,2$) are coefficients that vary minimally with Σ and f (Fig. 8 and Table III). Upon asperity contact, smaller values of λ obtain and are subject to further study.

A generalized expression for the total matrix crack opening u^T produced by the applied loads t and thermal stress $E_f\Delta\alpha\Delta T$ can also be obtained using the finite-element results as

$$u^T = a\Delta\alpha\Delta T(g_2 + g_1\tau_f) \tag{8a}$$

where

$$g_1 = \lambda_1(f,\Sigma) + \lambda_2(\Sigma)\frac{\ell}{a} \tag{8b}$$

$$g_2 = \lambda_3(f,\Sigma) + \lambda_4(\Sigma)\frac{\ell}{a} \tag{8c}$$

with λ_i ($i = 1,4$) given in Table III (see also Fig. 8). These results will be used below to discuss toughening.

IV. Fiber Cracking

Some understanding of *fiber cracking* can be achieved by estimating the strain energy release rates, $\mathcal{G}^k$, associated with a small kink crack in the fiber, at the end of the debond. For a kinked crack in a homogeneous elastic body ($\Sigma = 1$) the stress intensity factors at the kink, K_1 and K_2, are

$$K_1 = C_{11}K_I + C_{12}K_{II} \tag{9a}$$

$$K_2 = C_{21}K_I + C_{22}K_{II} \tag{9b}$$

where K_I and K_{II} refer to the primary crack and[10]

$$C_{11} = \frac{1}{4}\left(3\cos\frac{\beta}{2} + \cos\frac{3\beta}{2}\right) \tag{10a}$$

$$C_{12} = -\frac{3}{4}\left(\sin\frac{\beta}{2} + \sin\frac{3\beta}{2}\right) \tag{10b}$$

Table II. Energy Release Rate and Phase Angle Parameters for Residually Stressed Composites ($f = 0.2$), $\nu_f = \nu_m = 0.25$

E_m/E_f	C_1	C_2	C_3	C_4	k_1	k_2	k_3
0.4	0.174	0.021	−0.296	0.307	0.189	−0.280	0.152
1.0	0.278	0.110	−0.508	0.449	0.314	−0.370	0.200
2.5	0.388	0.235	−0.778	0.548	1.486	−0.430	0.228

$$C_{21} = \frac{1}{4}\left(\sin\frac{\beta}{2} + \sin\frac{3\beta}{2}\right) \tag{10c}$$

$$C_{22} = \frac{1}{4}\left(\cos\frac{\beta}{2} + 3\cos\frac{3\beta}{2}\right) \tag{10d}$$

with β being the kink angle (Fig. 9). The energy release rate $\mathcal{G}^k$ of the kink crack is thus

$$\mathcal{G}^k = \frac{1-\nu^2}{E}(K_1^2 + K_2^2)$$

$$= \frac{1-\nu^2}{E}[(C_{11}K_I + C_{12}K_{II})^2 + (C_{21}K_I + C_{22}K_{II})^2]$$

$$= \frac{1-\nu^2}{E}(a_1K_I^2 + a_2K_IK_{II} + a_3K_{II}^2) \tag{11}$$

or

$$\frac{\mathcal{G}^k}{\mathcal{G}^T} = \frac{a_1 + a_2\arctan(\psi) + a_3[\arctan(\psi)]^2}{1 + [\arctan(\psi)]^2} \tag{12}$$

where

$$a_1 = \frac{1}{8} + \frac{1}{2}\cos^2\frac{\beta}{2} + \frac{1}{4}\cos\beta + \frac{1}{8}\cos 2\beta$$

$$a_2 = -\sin\beta - \frac{1}{2}\sin 2\beta$$

$$a_3 = \frac{5}{8} + \frac{1}{2}\sin^2\frac{\beta}{2} + \frac{3}{4}\cos\beta - \frac{3}{8}\cos 2\beta$$

Differentiation to obtain the maximum in the *fiber* gives

$$\frac{d\mathcal{G}^k}{d\beta} = 0 \longrightarrow \frac{da_1}{d\beta}K_I^2 + \frac{da_2}{d\beta}K_IK_{II} + \frac{da_3}{d\beta}K_{II}^2 = 0 \tag{13}$$

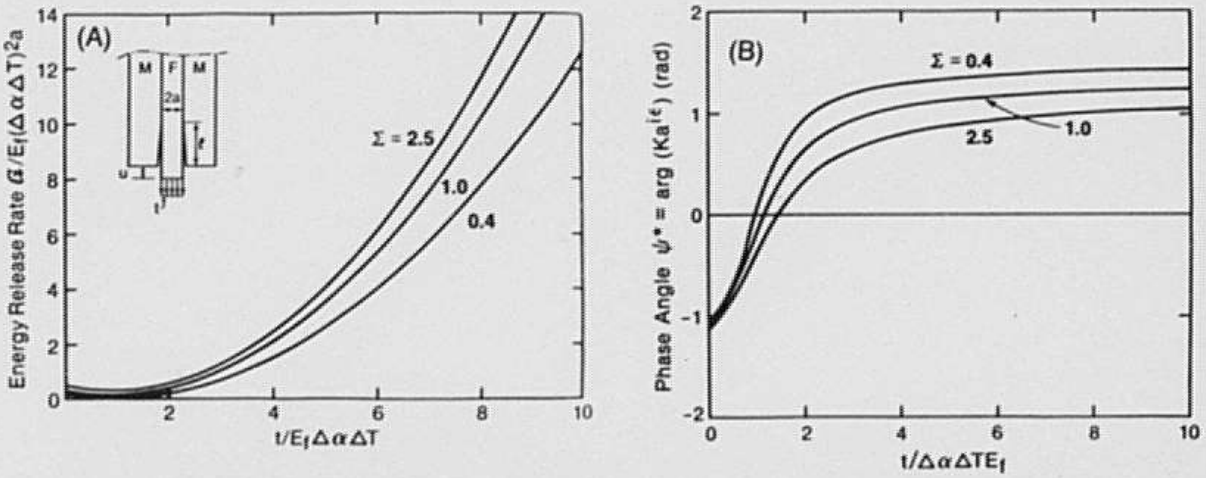

Fig. 7. (A) Variations in total nondimensional debond strain energy release rate with nondimensional applied stress for several elastic modulus ratios and fixed Poisson's ratios, $\nu_f = \nu_m = 0.25$. (B) Trends in phase angle with nondimensional stress for several elastic modulus ratios.

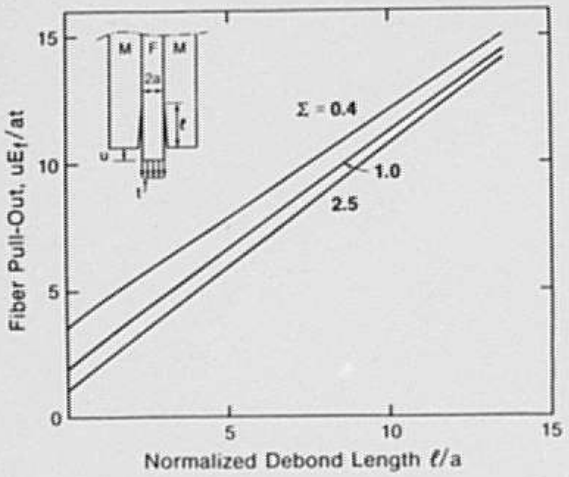

Fig. 8. Trends in nondimensional compliance with debond length for $f = 0.15$ and $\nu_f = \nu_m = 0.25$.

where

$$\frac{da_1}{d\beta} = -\frac{1}{2}\sin\beta(1 + \cos\beta)$$

$$\frac{da_2}{d\beta} = 1 - \cos\beta(1 + 2\cos\beta)$$

$$\frac{da_3}{d\beta} = -\frac{1}{2}\sin\beta(1 - 3\cos\beta)$$

The resultant maximum is plotted in Fig. 9. It is apparent that $\mathcal{G}$ for the kink crack is only slightly larger than that for the interface crack at all t, indicating that *debonds are not expected to cause fiber cracking*. This conclusion has been confirmed[11] by further studies for the general case, $\Sigma \neq 1$. The problem of fiber failure in the wake, as it relates to toughening, thus appears to be dominated by statistical considerations, as elaborated below.

V. Wake Debonding

The trends in $\mathcal{G}$ with the traction t exerted by the extending matrix crack provide insight concerning debonding in the crack wake. First, it is noted that for the case of tensile residual stress at the interface, the steady-state nature of $\mathcal{G}$ would cause the debond, once critical, to extend a considerable distance along the interface. However, in many cases such extensive debonding would be inhibited either by friction at asperities on the debond interfaces (which causes $\mathcal{G}$ to become smaller than indicated by the present calculations) or by fiber failure, as elaborated below. It is also evident from the nondimensional parameter $\mathcal{G}/E_f a(\Delta\alpha\Delta T)^2$ that debonding is more likely ($\mathcal{G}$ increases) as the fiber radius, the fiber stiffness, and the misfit strain increase. Furthermore, since $\mathcal{G}$ initially decreases upon fiber loading ($t > 0$), a threshold stress must be involved in debond extension in the crack wake. Specifically, $\mathcal{G}$ must at least exceed the value at $t = 0$ before the debond extends.

A quantitative assessment of debonding would require knowledge of the interface fracture locus $\mathcal{G}_{ic}(\psi)$ as well as the fiber bundle strength S_b, given by[12]

$$S_b = S_0(\ell/\ell_0)^{-1/m}(me)^{-1/m} \tag{14}$$

where S_0 and ℓ_0 are the scale parameters and m is the shape parameter, as governed by the fiber strength distribution. Specifically, the competition between debonding and fiber failure in the wake may be addressed if t in Eq. 6(*a*) is replaced by S_b (Eq. (14)) and $\mathcal{G}^T$ equated to $\mathcal{G}_{ic}$ at the relevant ψ. In particular, the magnitude of the debond length ℓ^* at which fiber failure occurs in preference to further debonding can be readily derived as

$$\ell^*/\ell_0 = \frac{(S_0/E_f\Delta\alpha\Delta T)^m}{me\left\{-\frac{k_2}{2k_3} + \frac{1}{2k_3}\left[k_2^2 + 4k_3\left(k_1 - \frac{\mathcal{G}_{ic}}{aE_f(\Delta\alpha\Delta T)^2}\right)\right]^2\right\}^m} \tag{15}$$

Debonding would proceed until ℓ reaches ℓ^*, whereupon fiber failure would occur. The actual locations of the fiber failures are given by statistical arguments.[4]

VI. Toughening

When the composite is subject to tensile residual stress at the interface, the present analysis has revealed that a *positive* mode I exists along the debond. Consequently, sliding and classical *pull-out* contributions to toughness only exist if the fibers are rough and friction is provided by asperity contact. In practice, fibers are not straight and debonded interfaces are not smooth.[1] A sliding resistance thus usually exists,[13] having magnitude governed by the frictional characteristic of the debonded interface.

When conditions of debonding without friction exist, the fibers primarily contribute to toughness through crack *bridging*. The bridging contribution to toughness can be derived from the compliance relations derived in Section III by noting that the asymptotic toughening is[14]

$$\Delta\mathcal{G}_b = 2f\int_0^{t=S} t(u)\,du \tag{16}$$

where S is the axial stress of which the fibers fail. This topic is elaborated elsewhere.[15]

Table III. Coefficients λ^i ($i = 1, 4$) Used in the Interpolation of the Matrix Crack Opening

	$\lambda_1(\Sigma, f)$							
Σ	$f = 0.05$	$f = 0.1$	$f = 0.2$	$f = 0.3$	$f = 0.4$	$f = 0.5$	$f = 0.6$	$f = 0.7$
0.4	3.22	3.42	2.04	1.76	1.55	1.40	1.28	1.19
1.0	1.85	1.96	1.30	1.14	1.00	0.87	0.75	0.63
2.5	0.96	1.01	0.72	0.64	0.57	0.49	0.41	0.30
	$-\lambda_4(\Sigma, f)$							
Σ	$f = 0.05$	$f = 0.1$	$f = 0.2$	$f = 0.3$	$f = 0.4$	$f = 0.5$	$f = 0.6$	$f = 0.7$
0.4	2.59	2.75	1.64	1.42	1.25	1.12	1.03	0.95
1.0	1.73	1.84	1.23	1.07	0.94	0.81	0.70	0.59
2.5	1.05	1.11	0.79	0.71	0.62	0.54	0.44	0.33

Σ	$\lambda_2(\Sigma)$	$-\lambda_4(\Sigma)$
0.4	0.838	1.062
1.0	0.910	1.058
2.5	0.964	1.043

Subsequent to fiber failure, some closure of the debond surface generally occurs and the pullout motion of the fibers is typically resisted by frictional contact at asperities, as expressed by a shear resistance, τ_i. Pullout then has a profound effect on the mechanical properties. This phenomenon intimately involves statistical considerations through the location of fiber failure.[4] However, fiber failure and pullout based on a *constant* shear resistance τ_i[4] is clearly an oversimplification, especially prior to fiber failure when asperity contact can be affected by opening of the debond surfaces. A more complete analysis of the pullout that incorporates these effects is in progress.

VII. Closure

The present article has provided rigorous solutions for the mechanics of debonded interfaces in composites with interfaces subject to residual tension. Steady-state behavior at the debonds has been demonstrated with a phase angle that depends sensitively on the residual/applied stress ratio and on the elastic properties of the fiber and the matrix. The results of this analysis have been used to derive conditions for fiber debonding in the crack wake, to ascertain fiber failure criteria pertinent to fiber pullout and toughening and to examine the role of debonding and residual stress in fiber bridging toughness.

The actual fiber response in the crack wake is undoubtedly more complex than the symmetrical debond configuration considered in the present analysis. However, debonding should proceed in a manner that restores symmetry, since asymmetric debonds are subject to antiplane shear as well as in-plane shear and opening. Consequently, while more complex calculations would be envisioned, it does not appear that additional insight would emerge.

APPENDIX A

Crack Front Debonding

In a composite containing fibers with partial thermal debonds (Fig. A1), growth of the debonds can occur upon passage of the matrix crack. Specifically, the debond experiences a biaxial stress, in-plane strain, from the approaching matrix crack given by

$$\sigma_{xx} = \frac{K_m}{\sqrt{2\pi r}} \tag{A-1a}$$

$$\sigma_{zz} = \frac{2\nu K_m}{\sqrt{2\pi r}} \tag{A-1b}$$

where K_m is the matrix toughness, and r is the distance from the crack front. The stress-intensity factors at a debond subject to biaxial stress σ are[16] ($\Sigma = 1$)

$$\frac{K_I}{\sigma\sqrt{\pi a}} = \frac{\left[\frac{1}{2}\sin\alpha(1+\cos\alpha)\right]^{1/2}}{1+\frac{1}{2}\sin^2\alpha} \tag{A-2a}$$

$$\frac{K_{II}}{\sigma\sqrt{\pi a}} = \frac{\left[\frac{1}{2}\sin\alpha(1-\cos\alpha)\right]^{1/2}}{1+\frac{1}{2}\sin^2\alpha} \tag{A-2b}$$

where 2α is the angle included by the debond (Fig. A1). The modulus of K is thus

$$\frac{|K|}{\sigma\sqrt{\pi a}} = \frac{\sin\frac{1}{2}\alpha}{1+\frac{1}{2}\sin^2\alpha} = g(\alpha) \tag{A-3}$$

where $g(\alpha)$ is plotted in Fig. A1. Noting that σ derives from both the crack tip field and the residual stress q gives

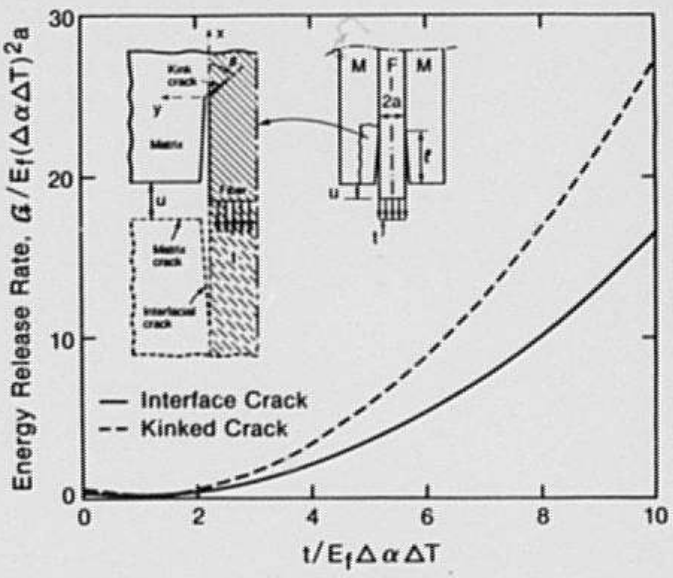

Fig. 9. Variations in nondimensional maximum energy release rate for a kink crack, with nondimensional applied stress; homogeneous system ($\Sigma = 1$); comparison with '6'.

$$\sigma = q + \frac{1}{2}(\sigma_{xx} + \sigma_{zz}) \tag{A-4}$$

whereupon Eq. (A-3) becomes

$$\frac{|K|}{g(\alpha)} = q\sqrt{\pi a} + \frac{1+2\nu}{2\sqrt{2}}K_m\sqrt{\frac{a}{r}} \tag{A-5}$$

The quantity $|K|$ attains a maximum as $r \to a$. While not strictly valid in this limit, it is insightful to obtain the maximum from Eq. (A-5) as

$$\frac{|K|_{max}}{K_m g(\alpha)} = \frac{q\sqrt{\pi a}}{K_m} + \frac{1+2\nu}{2\sqrt{2}} \tag{A-6}$$

It is apparent from the functional form of $g(\alpha)$ depicted in Fig. A1 that a *lower bound* condition exists below which debonding cannot occur. This condition involves the peak value of $g(\alpha)$ that occurs when $\alpha \approx 0.3\pi$

$$\hat{g}(\alpha) = 0.76 \tag{A-7}$$

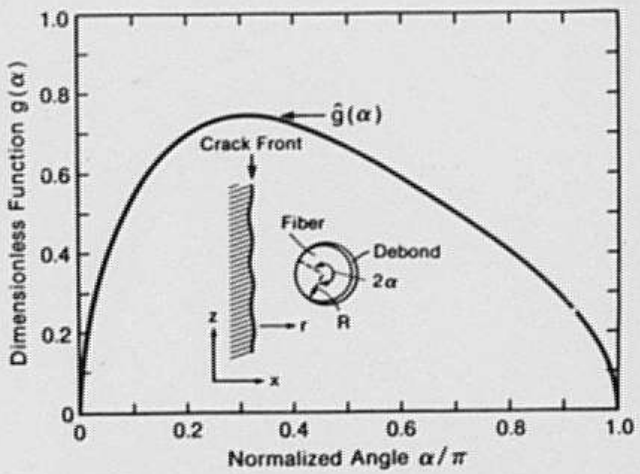

Fig. A1. Normalized modulus $|K|$ of the stress intensity factor at fiber thermal debonds due to the presence of the matrix crack.

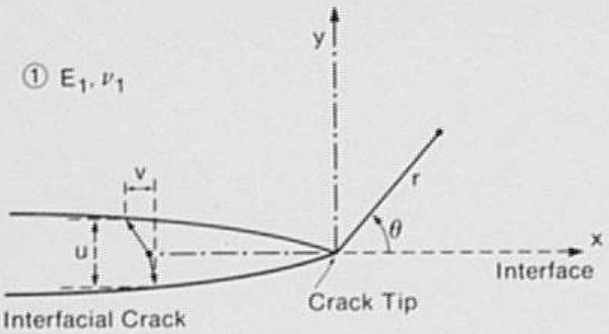

Fig. B1. Displacement field associated with a crack at a bimaterial interface.

Consequently, by equating $|K|_{max}$ to the fracture resistance of the interface $|K_c|(\psi)$, the lower bound debonding condition becomes

$$\frac{|K_c|(\psi)}{K_m} < 0.76\left(\frac{1+2\nu}{2\sqrt{2}} + \frac{q\sqrt{\pi a}}{K_m}\right) \tag{A-8}$$

This result is used in Section V to conclude that wake debonding is preferable to fiber failure at the end of the debond (recognizing that the critical values of K for the fiber and matrix are typically of similar magnitude).

Another important feature of the debonding problem evident from Fig. A1 is the realization that complete circumferential debonding is unlikely to occur, because $g(\alpha) \to 0$ as $\alpha \to \pi$. Consequently, the matrix crack is unlikely to encounter a fully debonded fiber. This realization emphasizes the importance of the conclusions reached in Section V that wake debonding occurs more readily than fiber failure when condition (A–8) is satisfied.

An analysis similar to that presented in this appendix has been independently conducted by Nix.[17]

APPENDIX B

Mechanics of Interface Cracks

The small strain linear elasticity singularity solution in the crack tip region can be developed using the bimaterial constant ε, which for plane strain is defined following Rice and Sih[5] and Rice[6] as

$$\varepsilon = \frac{1}{2\pi}\ln\frac{1+\beta}{1-\beta} \tag{B-1}$$

where

$$\beta = -\frac{1}{2}\left[\frac{G_1}{G_2}(1-2\nu_2) - (1-2\nu_1)\right] \Big/ \left[\frac{G_1}{G_2}(1-\nu_2) + (1-\nu_1)\right]$$

is one of the plane strain Dundurs parameters[18] and G_i and ν_i $(i = 1, 2)$ are the shear modulus and Poisson's ratio for materials 1 and 2, respectively. The traction at a distance r ahead of the crack tip is then given by

$$\sigma_{22} + i\sigma_{12} = \frac{K}{\sqrt{2\pi r}} r^{i\varepsilon} \tag{B-2}$$

where $i = \sqrt{-1}$ and $K = \text{Re}\,(K) + i\,\text{Im}\,(K)$ is the complex stress intensity factor introduced by Rice[6] and Hutchinson *et al.*[19] Furthermore, the relative plane strain displacements of two points at distance r behind the crack tip on the top and bottom crack surfaces, Δu_x and Δu_y (Fig. B1), are also given in terms of the complex K and the bimaterial constant ε as follows:

$$\Delta u_y + i\Delta u_x = \frac{2\left(\frac{1-\nu_1}{G_1} + \frac{1-\nu_2}{G_2}\right)K}{(1+2i\varepsilon)\cosh(\pi\varepsilon)}\sqrt{\frac{r}{2\pi}}\, r^{i\varepsilon} \tag{B-3}$$

The energy release rate per unit of new crack area $\mathcal{G}$ in terms of the complex stress intensity factor K is

$$\mathcal{G} = \frac{\frac{1-\nu_1}{G_1} + \frac{1-\nu_2}{G_2}}{4\cosh^2(\pi\varepsilon)}|K|^2 \tag{B-4}$$

where $|K|^2 = K\bar{K}$ is the modulus of the complex stress intensity factor, K.

The complex stress intensity factor K can be expressed in terms of its modulus $|K|$ and phase angle ψ:

$$K = |K|e^{i\psi} \tag{B-5}$$

When all complex quantities are expressed in polar form, Eq. (B–3) yields an expression for the phase angle ψ, such that

$$\psi = \phi + B - \varepsilon \ln r \tag{B-6}$$

where $\phi = \arctan(\Delta u_x/\Delta u_y)$ and $B = \arctan(2\varepsilon)$ are both nondimensional, whereas the $\varepsilon \ln r$ term is unit sensitive. This peculiarity of the phase angle has been recently examined by Rice[6] with the conclusion that ψ provides a proper characterizing parameter, provided that lengths are measured using consistent units (typically micrometers). While it is important to use ψ to describe fracture data, it is convenient to present calculated phase angles using a scale-invariant form:

$$Ka^{i\varepsilon} = |K|e^{i\psi^*} \tag{B-7}$$

where $\psi^* = \psi + \varepsilon \ln a$ with a being a characteristic dimension, in this case the fiber radius.

APPENDIX C

A known finite-element solution to a linear elastic boundary value problem which involves a crack with traction-free surfaces can be used in conjunction with Parks' stiffness derivative method[20] to evaluate with sufficient accuracy the associated energy release rate $\mathcal{G}$.[21] In summary, $\mathcal{G}$ is given by

$$\mathcal{G} = -\frac{1}{2}\sum_{n=1}^{\text{No. of elements}} \{u_N\}^T \frac{\partial[S]}{\partial \ell}\{u_N\} \tag{C-1}$$

where $\{u_N\}$ denotes the nodal displacement vector, $[S]$ the stiffness matrix, and $\partial/\partial\ell$ differentiation with respect to crack length. The symbol Σ implied summation over all the distorted elements during the virtual crack extension. The method is still valid in the case of bimaterial crack problems as long as the crack surfaces remain traction free.

Consider a bimaterial problem for which it is desired to compute Re (K) and Im (K). First, solve the boundary value problem by the finite-element method and find $\{u_N\}$. From this, compute $\mathcal{G}$ by the virtual crack extension technique summarized by Eq. (C–1). Then add to $\{u_N\}$ the displacements $\{\Delta u_N^1\}$ for a problem in the same geometry but for which Im $(K) = 0$ and Re $(K) = \Delta$ Re (K).

A new value $\mathcal{G} + \Delta_1\mathcal{G}$ can now be obtained through Eq. (C–1) for the nodal displacements $\{u_N + \Delta u_N^1\}$. The result for this calculation can be shown to be such that the change in the value of $\mathcal{G}$ is

$$\Delta_1\mathcal{G} = \frac{1}{H}[\Delta\,\text{Re}\,(K)^2 + 2\,\text{Re}\,(K)\Delta\,\text{Re}\,(K)] \tag{C-2}$$

Solving for Re (K) gives

$$\text{Re}\,(K) = \frac{H}{2}\frac{\Delta_1 \mathcal{G}}{\Delta\,\text{Re}\,(K)} - \frac{1}{2}\Delta\,\text{Re}\,(K) \qquad \text{(C-3)}$$

The second term can be neglected compared with the first if $\Delta\,\text{Re}\,(K)^2$ is selected to be small. The procedure can be repeated for an added vector $\{\Delta u_N^{II}\}$ such that $\text{Re}\,(K) = 0$ and $\text{Im}\,(K) = \Delta\,\text{Im}\,(K)$, in which case an expression for $\text{Re}\,(K)$ can also be derived.

The vectors $\{\Delta u_N^{I}\}$ and $\{\Delta u_N^{II}\}$ comprise sets of virtual displacements and can represent any problem. Furthermore, it should be noted that the virtual field is needed only for the nodes associated with the distorted ring of elements. In view of this, the asymptotic crack tip displacements can be used everywhere as a suitable field.

When $\text{Im}\,(K) = 0$ and $\text{Re}\,(K) = \Delta\,\text{Re}\,(K)$

$$\Delta u_j^{I} = \frac{\Delta\,\text{Re}\,(K)}{2G_j}\sqrt{\frac{r}{2\pi}}\frac{e^{\pi\varepsilon}}{1+e^{2\pi\varepsilon}} f^{I}(r,\theta,\varepsilon,\mu_j) \qquad \text{(C-4)}$$

whereas when $\text{Re}\,(K) = 0$ and $\text{Im}\,(K) = \Delta\,\text{Im}\,(K)$

$$\Delta u_j^{II} = \frac{\Delta\,\text{Im}\,(K)}{2G_j}\sqrt{\frac{r}{\pi}}\frac{e^{\pi\varepsilon}}{1+e^{2\pi\varepsilon}} f^{II}(r,\theta,\varepsilon,\mu_j) \qquad \text{(C-5)}$$

where

$$f_x^{I}(r,\theta,\varepsilon,\mu_j) = D_j + 2\delta_j \sin\theta \sin\phi$$

$$f_y^{I}(r,\theta,\varepsilon,\mu_j) = -C_j - 2\delta_j \sin\theta \cos\phi$$

$$f_x^{II}(r,\theta,\varepsilon,\mu_j) = -C_j + 2\delta_j \sin\theta \cos\phi$$

$$f_y^{II}(r,\theta,\varepsilon,\mu_j) = -D_j + 2\delta_j \sin\theta \sin\phi$$

The constants C_j, D_j, δ_j, and ϕ are functions of the material constants and location in the continuum. They are given as follows:

$$\delta_1 = e^{-(\pi-\theta)\varepsilon}$$

$$\delta_2 = e^{+(\pi+\theta)\varepsilon}$$

$$\phi = \varepsilon \ln r + \frac{\theta}{2}$$

$$C_j = \overline{\beta}\gamma_j \cos\frac{\theta}{2} - \beta\overline{\gamma}\sin\frac{\theta}{2}$$

$$D_j = \beta\gamma_j \cos\frac{\theta}{2} + \overline{\beta}\,\overline{\gamma}\sin\frac{\theta}{2}$$

$$\beta = \frac{0.5\cos(\varepsilon \ln r) + \varepsilon \sin(\varepsilon \ln r)}{0.25 + \varepsilon^2}$$

$$\overline{\beta} = \frac{0.5\sin(\varepsilon \ln r) - \varepsilon \cos(\varepsilon \ln r)}{0.25 + \varepsilon^2}$$

$$\gamma_j = \mu_j\delta_j - \frac{1}{\delta_j}$$

$$\overline{\gamma}_j = \mu_j\delta_j + \frac{1}{\delta_j}$$

Also

$$\gamma_j = \begin{cases} 3 - 4\nu_j & \text{plane strain} \\ (3-\nu_j)/(1+\nu_j) & \text{plane stress} \end{cases}$$

In the above equations, j is a material index which takes the values 1 and 2 for materials 1 and 2, respectively (Fig. B1).

Acknowledgment: Useful discussions with L. S. Sigl are acknowledged.

References

[1] E. Bischoff, M. Rühle, O. Sbaizero, and A. G. Evans, "Microstructural Studies of the Interfacial Zone of a SiC-Fiber-Reinforced Lithium Aluminun Silicate Glass-Ceramic," *J. Am. Ceram. Soc.*, **72** [5] 741–45 (1989).

[2] M. D. Thouless, O. Sbaizero, L. S. Sigl, and A. G. Evans, "Effect of Interface Mechanical Properties on Pullout in a SiC-Fiber-Reinforced Lithium Aluminum Silicate Glass-Ceramic," *J. Am. Ceram. Soc.*, **72** [4] 525–32 (1989).

[3] A. G. Evans, "The New Generation of High Toughness Ceramics"; to be published in ASTM Special Technical Publication, Fracture Mechanics.

[4] M. D. Thouless and A. G. Evans, "Effects of Pull-out on the Toughness of Reinforced Ceramics," *Acta Metall.*, **36**, 517 (1988).

[5] J. R. Rice and G. C. Sih, "Plane Problems of Cracks in Dissimilar Media," *J. Appl. Mech.*, **32**, 418–23 (1965).

[6] J. R. Rice, "Elastic Fracture Mechanics for Interfacial Cracks," *J. Appl. Mech.*, **55**, 98 (1988).

[7] P. G. Charalambides, J. Lund, R. M. McMeeking, and A. G. Evans, "A Test Specimen for Determining the Fracture Resistance of Bimaterial Interfaces"; to be published in *J. Appl. Mech.*

[8] J. W. Hutchinson and A. G. Evans, "On the Mixed Mode Fracture Resistance of Interfaces," *Acta Metall.*, **37** [3] 909–16 (1989).

[9] P. P. L. Matos, R. M. McMeeking, P. G. Charalambides, and M. D. Drory, "A Method for Calculating Stress Intensities in Bimaterial Fracture"; to be published in *Int. J. Fract.*

[10] B. Cotterell and J. R. Rice, "Slightly Curved or Kinked Cracks," *Int. J. Fract.*, **16**, 155 (1980).

[11] M. He and J. W. Hutchinson, Harvard Report, MECH-119, Cambridge, MA, April 1988.

[12] H. T. Corten; p. 27 in Modern Composite Materials. Edited by L. J. Broutman and R. H. Krock. Addison-Wesley, New York, 1967.

[13] D. B. Marshall and A. G. Evans, "Failure Mechanisms in Ceramic-Fiber/Ceramic-Matrix Composites," *J. Am. Ceram. Soc.*, **68** [5] 225–31 (1985).

[14] A. G. Evans and R. M. McMeeking, "On the Fracture Toughness of Strong Reinforcements," *Acta Metall.* **34**, 2435 (1986).

[15] P. G. Charalambides, "Toughening Caused by Elastic Bridging of Debonded Fiber"; unpublished work.

[16] G. C. Sih, Handbook of Stress Intensity Factors. Lehigh University Press, Bethlehem, PA, 1972.

[17] W. D. Nix, unpublished research presented at the Winter Study Group, Santa Barbara, CA, Jan. 1988.

[18] J. Dundurs, "Discussion," *J. Appl. Mech.*, **36**, 650–52 (1969).

[19] J. W. Hutchinson, M. E. Mear, and J. R. Rice, "Crack Paralleling on Interface Between Dissimilar Materials," *J. Appl. Mech.*, **53**, 828–32 (1987).

[20] D. M. Parks, "A Stiffness Derivative Finite Element Technique for Determination of Elastic Crack Tip Stress Intensity Factors," *Int. J. Fract.*, **10**, 487–502 (1974).

[21] J. R. Rice, "Mathematical Analysis in the Mechanics of Fracture"; pp. 191–311 in Fracture, An Advance Treatise. Edited by H. Liebowitz. Academic Press, New York, 1968. ❑